Article

Not peer-reviewed version

Integrated Analysis of Methane Cycles and Trends at the WMO/GAW Station of Lamezia Terme (Calabria, Southern Italy)

Francesco D'Amico *, Ivano Ammoscato, Daniel Gullì, Elenio Avolio, Teresa Lo Feudo, Mariafrancesca De Pino, Paolo Cristofanelli, Luana Malacaria, Domenico Parise, Salvatore Sinopoli, Giorgia De Benedetto, Claudia Roberta Calidonna *

Posted Date: 19 July 2024

doi: 10.20944/preprints202407.1587.v1

Keywords: methane; wind parameters; GAW; Lamezia Terme; Calabria; Southern Italy

Article

Integrated analysis of methane cycles and trends at the WMO/GAW station of Lamezia Terme (Calabria, Southern Italy)

Francesco D'Amico [1,2,*], Ivano Ammoscato [1], Daniel Gullì [1], Elenio Avolio [1], Teresa Lo Feudo [1], Mariafrancesca De Pino [1], Paolo Cristofanelli [3], Luana Malacaria [1], Domenico Parise [1], Salvatore Sinopoli [1], Giorgia De Benedetto [1] and Claudia Roberta Calidonna [1,*]

[1] National Research Council of Italy – Institute of Atmospheric Sciences and Climate, Area Industriale Comp. 15, I-88046 Lamezia Terme, Catanzaro, Italy; i.ammoscato@isac.cnr.it, d.gulli@isac.cnr.it, e.avolio@isac.cnr.it, t.lofeudo@isac.cnr.it, m.depino@isac.cnr.it, l.malacaria@isac.cnr.it, d.parise@isac.cnr.it, s.sinopoli@isac.cnr.it, g.debenedetto@isac.cnr.it, claudiaroberta.calidonna@cnr.it

[2] University of Calabria - Department of Biology, Ecology and Earth Sciences, Via Bucci Cubo 15B, 8-87036 Rende, Cosenza, Italy

[3] National Research Council of Italy – Institute of Atmospheric Sciences and Climate, Via P. Gobetti 101, I-40129 Bologna, Italy; p.cristofanelli@isac.cnr.it

* Correspondence: f.damico@isac.cnr.it, francesco.damico@unical.it

Abstract: Due to its high short-term global warming potential (GWP) compared to carbon dioxide, methane (CH_4) is a considerable agent of climate change. This research is aimed at analyzing data on methane gathered at the GAW (Global Atmosphere Watch) station of Lamezia Terme (Calabria, Southern Italy) spanning seven years of continuous measurements (2016-2022) and integrating the results with key meteorological data. Compared to previous studies on detected methane mole fractions at the same station, daily-to-yearly patterns have become more prominent thanks to the analysis of a much larger data set. Overall, the yearly increase of methane at the Lamezia Terme station is in general agreement with global measurements by NOAA, though local peaks are present, and an increase linked to Covid-19 is identified. Seasonal changes and trends have proved to be fully cyclic, with the daily cycles being largely driven by local wind circulation patterns and synoptic features. Outbreak events have been statistically evaluated depending on their weekday of occurrence to test possible correlations with anthropic activities. A cross analysis between methane peaks and specific wind directions has also proved that local sources may be deemed responsible for the highest mole fractions.

Keywords: methane; wind parameters; GAW; Lamezia Terme; Calabria; Southern Italy

1. Introduction

Methane (CH_4) is the simplest among alkanes and, thanks to its capacity to absorb terrestrial infrared radiation in a band at the 1.7, 2.3, 3.3 and 7.6 μm marks [1], is subject to monitoring due to its extremely high GWP (Global Warming Potential) as a GHG (greenhouse gas), which is 84-87 times higher than that of CO_2 for the time span of two decades [2]. Methane's GWP-100 value (GWP in a century) drops to 27 compared to CO_2 [3] and is much less persistent in the atmosphere, thus falling in the short-lived climate forcers (SLCF) category, along with ozone and aerosols [2]. Atmospheric concentrations of methane in the atmosphere have experienced a sharp rise since the beginning of the industrial period, a rise that is well established in scientific research ever since the late 1990s [4] and recently broke the 150% increase threshold over pre-industrial era levels [5]. With a calculated global mean value of approximately 700 ppb in the year 1750 which is almost three times lower than the 2022 observed global mean of 1911,9 ppb [6], the increase of methane in the atmosphere is largely due to anthropic activities [7,8]. On a global scale, this compound has been measured by NOAA's

 doi:10.20944/preprints202407.1587.v1

Earth System Research Laboratory ever since 1983 so the data from that point onward is deemed particularly reliable and helps defining medium term trends [9]. Methane has also proved to drive climate change by the means of several side effects to the chemistry of Earth's atmosphere, such as the production of H_2O in the stratosphere and the release of O_3 (ozone) in the troposphere [2]. Although methane concentrations are two orders of magnitude lower compared to those of carbon dioxide, the high GWP of this compound has sparked notable interest in the scientific community and is now widely regarded as one of the main causes of climate change [10–12].

Estimates on present-day methane releases, uptake and sinks have several degrees of uncertainty [13], but improvements in predictive models over the past few years have helped to somehow constrain these estimations. Globally, according to the IEA report from 2021 [14], the annual emissions of methane – both natural and anthropogenic – are approximately 570 Tg (teragrams, 10^{12} grams), though some estimates are as high as 737 Tg [12]. Geologic releases account for 43–50 Tg y^{-1} [15], while the broad anthropogenic emissions are in the 360 Tg y^{-1} range, 110-128 Tg of which are related to pure fossil fuel burning [12]. Speaking of some of the most notable sources, wetlands contribute with 101–179 Tg y^{-1} [12], biomass burning estimates are as high as 30 Tg y^{-1} [12], livestock releases account for an estimated 95–109 Tg y^{-1}, 87–97 Tg of which are directly linked to enteric fermentation processes [16], and termites are deemed responsible for 15 Tg y^{-1} worth of emissions [17]. In the past few years, the nature and characteristics of geologic emissions have been further divided and classified into several sub-categories, depending on the sources and mechanisms that drive said releases [15]. These categories are now fully recognized by IPCC reports. Overall, it is now estimated that 40% of methane emissions are natural, while the remaining 60% are anthropogenic [12].

Sinks and uptake phenomena remove approximately 630 Tg of methane from the atmosphere each year [10], but the amount is variable over time [12]. It's worth noting that the geographical distribution of excessive methane emissions is asymmetric, with the northern hemisphere yielding higher values compared to the southern hemisphere, and broad seasonal cycles have also been observed even before the age of NOAA's Earth System Research Laboratory enhanced detections [18]. Additionally, soil uptake of methane in tropical and temperate forests of the southern hemisphere is higher than that of their northern counterparts [19]. The overall upward trend in atmospheric concentration is attributable to the excess in anthropogenic emissions compared to natural sinks [10], though the phenomenon of methane variability in Earth's atmosphere is much more complicated compared to that of CO_2: for instance, an anomalous drop in atmospheric methane was recorded in 2004 [20], with the whole 1983-2006 observation streak reporting a downward trend in annual growth rates [21–23]. Methane has been on a nearly constant rise ever since that sudden drop, but the isotopic $^{13}C/^{12}C$ ratio ($\delta^{13}C$) began to decrease after two centuries of regular increase, highlighting a major shift in fractionation processes induced by different sinks [5,24]. Isotopic ratios aside, a well above average increase was recorded in 2020, attributable to the Covid-19 pandemic [25]. Overall, while the trends and mechanisms that drive CO_2 increases in the atmosphere are very well defined, those of CH_4 are still somewhat puzzling to climate scientists and researchers [26], hence the need of more detailed analyses on this compound.

This research provides unprecedented detail on methane cycles and trends as detected by a World Meteorological Organization/Global Atmosphere Watch (WMO/GAW) LMT observatory in Calabria (Southern Italy) over a period of seven years, from 2016 to 2022. The second section will describe the observation site and its characteristics, while the third section will report information on datasets and methods used to process data. The results are shown in the fourth section, followed by discussion, conclusions and perspectives on future research studies. Supplementary Materials cover graphs and tables not shown in the main text.

2. The Lamezia Terme CNR-ISAC Observatory

The Lamezia Terme site (WMO/GAW code: LMT) is a coastal station located in Calabria, Southern Italy, more precisely in the Sant'Eufemia plain (Lat: 38.88 °N; Lon: 16.23 °E; Alt: 6m above sea level), south of Lamezia Terme. The observatory, fully operated by the National Research Council

 doi:10.20944/preprints202407.1587.v1

of Italy – Institute of Atmospheric Sciences and Climate (CNR-ISAC), is located approximately 600 meters from the Tyrrhenian coastline of Calabria, and officially started its data gathering operations in 2015. It has since provided continuous data on several chemical and meteorological parameters. Wind characteristics at this coastal site were analyzed in the past [27]. Due to the geographic location of the experimental site, winds coming from the northeast are more subject to anthropic influence while winds coming from the west, largely influenced by the sea, yield lower concentrations in pollutants, as clearly demonstrated in an earlier study [28]. The 10/28 (100-280° N) magnetic bearing of the runway in use at the nearby Lamezia Terme International Airport (IATA: SUF; ICAO: LICA) located 3 kilometers north from the observatory is also a tangible proof of the applicability of wind studies in the area. In fact, airports are built and designed with local wind circulation in mind.

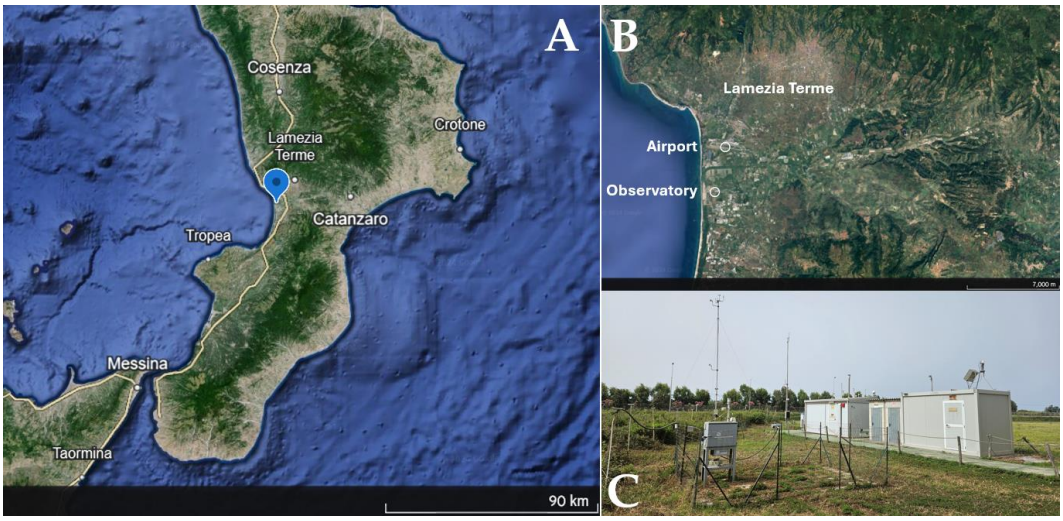

Figure 1. A: The location of Lamezia Terme's station within the region of Calabria, Southern Italy. B: Details of the Lamezia Terme municipal area, with notes on the location of the observatory and the airport. C: Details of the LMT observatory, where all instruments are located.

Ever since it started operations, LMT reported methane concentrations that may be attributable to several nearby sources, hence the concept of "multisource" site. Cristofanelli et al. (2017) [28], accounting for one year of data gathering, indicated the nearby Lamezia Terme International Airport and local livestock farming as two possible explanations for the observed peaks in methane, in addition to the anthropic pollution from nearby urban areas that is channeled towards the observatory when winds are coming from the northeast, as well as the A2 highway (part of the European route E45) located nearby.

From a climatological point of view, the area is known to be affected by seasonal changes to wind circulation. The study area, due its geographical location, is mainly affected by breeze circulation, as assessed by several works.

Federico et al. (2010a) [27] in studying the characteristics and importance of breezes, demonstrates how they dominate the local circulation and play a major role in the local climate. The authors observed relevant changes in average wind speeds over the seasons, as well as slight changes in wind orientation, though the general W-WSW/NE-ENE axis is dominant throughout the whole year and is deemed the result of wind channeling through the Marcellinara gap, which is the narrowest point in the entire Italian peninsula. When the 850 hPa layer is considered, the preferred orientation switches to a prevailing NW direction, which is consistent with large scale circulation in the area. Federico et al. (2010b) [29] further analyzed the nature of breeze circulations, considering two years of observation and modeling analyses, concluding that during spring, summer and part of fall, diurnal breeze circulation is considered as a combination of local and large-scale flows, while large-scale forcing represents a main driver of diurnal circulation in winter, November included, and nocturnal flows are believed to be due to the circulation of nocturnal breezes.

The confirmation on the presence of breeze and the influence of local conditions were both confirmed by further studies such as Gullì et al. (2017) [30] via the analysis of wind–lidar profiles for

 doi:10.20944/preprints202407.1587.v1

two continuous years. Figure 2 shows wind profiles accounting for multiple altitude thresholds, from 10 up to 300 meters, collected by a Zephir lidar 300 at the LMT observation site.

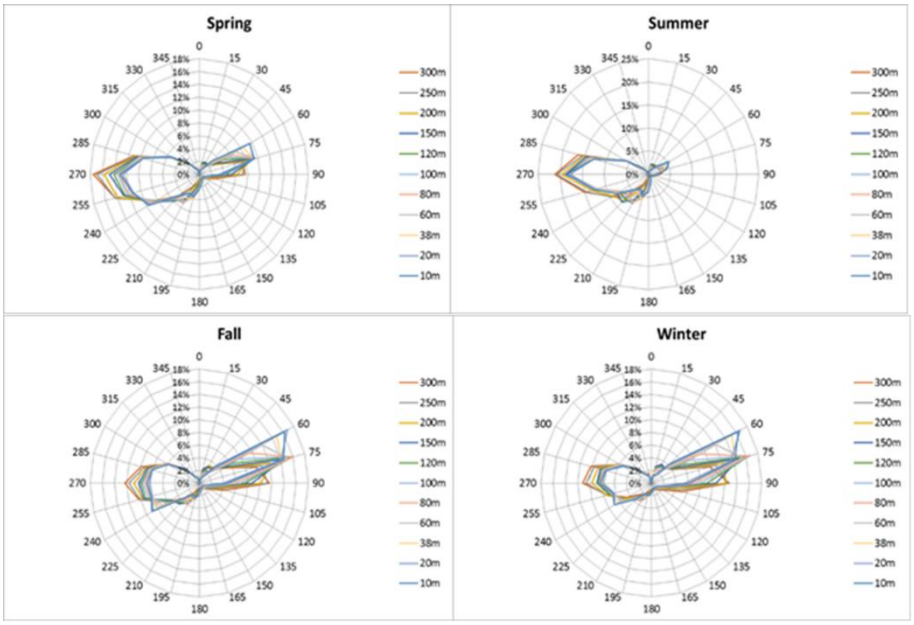

Figure 2. Seasonal wind roses at all levels during the 2014-2016 period, divided by thresholds between 10 and 300 meters, and collected by Zephir Wind Lidar. From Gullì et al. (2017) [30].

In a recent work, Lo Feudo et al. (2020) [31] studied the characteristics of the vertical structure of the Planetary Boundary Layer at the LMT site during an experimental campaign carried out in July/August 2009. The integration of different instruments (surface stations, wind profiler, Lidar, Sodar) with high resolution weather model products allowed to further assess the roles played by sea breeze and synoptic flows in the area.

Due to its location in the articulated context of the Mediterranean and, specifically, in the narrowest corridor of the Italian peninsula, the LMT station is subject to the exposure to open fire emissions, as recently reported in Malacaria et al. (2024) [32], and frequent Saharan dust events [33].

3. Instruments, Datasets, and Methods

Methane data has been gathered continuously using Picarro G2401 detectors (California, USA), which rely on the CRDS (Cavity Ring-Down Spectrometry) principle to estimate the concentrations in parts per million (ppm) of CO_2 (carbon dioxide), CH_4, CO (carbon monoxide) and H_2O (water vapor, as a percentage). The detectors have been subject to periodic calibration during the entire observation period. This research study is based on average data aggregated on an hourly basis, also accounting for the standard deviation of aggregated data as a stability indicator. Methane concentrations are shown in ppb (parts per billion) throughout all graphs and tables in this paper.

An automatic weather station (Vaisala WXT520, Finland) measured at 10m ASL the following meteorological parameters: temperature, relative humidity, wind speed and direction, pressure, and rain (10 averaged minutes). For the purposes of this research, wind speed and wind directions have been considered, which are measured by the WXT520 instrument via ultrasound. Wind data, just like in the previous case, has been aggregated on an hourly basis featuring the standard deviation as a data stability indicator.

Table 1 shows the coverage of available methane data compared to the total amount of hours elapsed between January 1st 2016 and December 31st 2022 (61368). Overall, of the 61368 elapsed hours, 57990 (94,49%) have been covered by verified and calibrated methane detections. This dataset will be referred to as "primary" throughout the paper. Three years out of seven have a total coverage rate exceeding 95%. Please note that both 2016 and 2020 are leap years, with extra 24 hours each (8784 hours instead of 8760).

 doi:10.20944/preprints202407.1587.v1

Table 1. Main coverage parameters (expressed as percentage of total actual hours per year) of the entire data set spanning seven years of continuous observations at LMT are shown in this table. Also reported is the coverage rate per year, with a maximum total coverage of 99,57% in 2017, and a minimum coverage of 83,83% in 2022. The second column shows the integration of Picarro G2401 and Vaisala WXT520 data satisfying the condition where both instruments were reliably operating at the same time.

Year	Picarro coverage (%)	Picarro – Vaisala (%)
2016	94,92%	92,2%
2017	99,57%	93,37%
2018	94%	74,68%
2019	97,6%	97,57%
2020	93,8%	93,79%
2021	97,71%	97,46%
2022	83,83%	75,41%
	94,49%[1]	89,07%[1]

[1] Total coverage.

Table 1 also reports the overall coverage of Picarro G2401 and Vaisala WXT520 data compared to the actual number of hours of the entire observation period. Data analysis involving both chemical data on methane and meteorological wind data was based on a subset of the main database where both instruments were fully operating at the same time. This, by definition, led to a slightly smaller "secondary" dataset available for cross-analyses of this particular kind. Five out of seven years have a combined integrated data coverage of more than 90%.

Finally, the two datasets have been processed in R 4.4.0 via ggplot2, ggpubr, tidyverse and openair packages, as well as their respective libraries. Depending on the goal of analysis, data have also been aggregated on monthly and seasonal basis (JFD = December, January, February for Winter; MAM = March, April, May for Spring; JJA = June, July, August for Summer; SON = September, October, November for Fall). Yearly, monthly and hourly aggregations have also been computed.

4. Results

4.1. General Monthly Trend

The more robust data set compared to previous research [28] highlights more long-term trends and cycles. Figure 3 shows monthly aggregated averages where seasonal trends, as well as a general upward trend, can be noticed. The 1st and 3rd quartiles are also plotted in Figure 3. Higher values are generally linked to Winter and Fall seasons, while Summer and Spring seasons yield the lowest values per year.

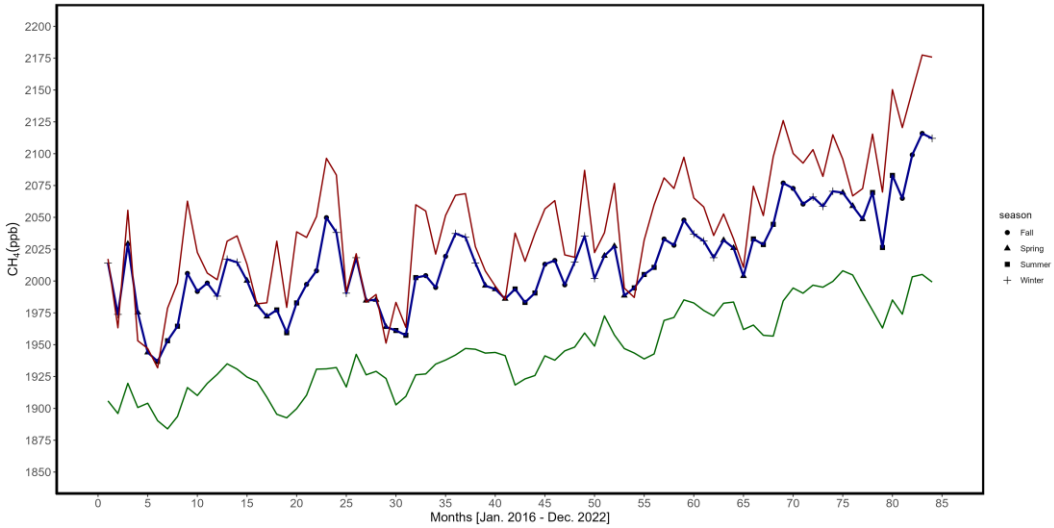

 doi:10.20944/preprints202407.1587.v1

Figure 3. Monthly averages accounting for the entire 2016-2022 period (84 months), shown in dark blue. Dark red and dark green show 3rd and 1st quartile trends, respectively. The four shapes are generated on a per-season basis.

4.2. Daily Cycle

With respect to daily cycles, intended as variations over the course of 24 hours, Figure 4 shows the hourly variation of methane mole fractions. The figure shows seasonal 2019 data specifically, as it's the year with the highest degree of integrated methane and wind data coverage (97,57%, see Table 1). Data are from the primary dataset. Table 2 reports the average values per hour, divided by season, as well as the standard deviations computed during data evaluation.

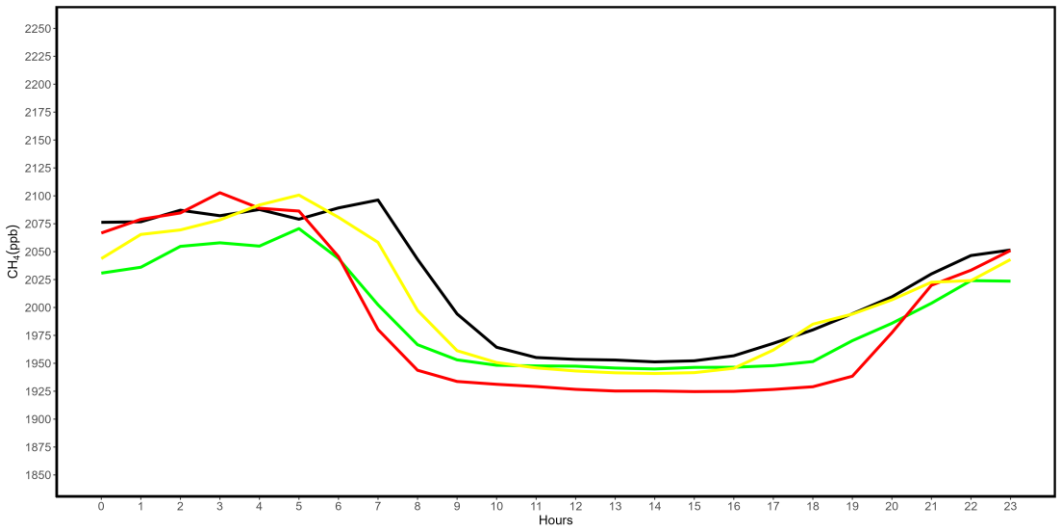

Figure 4. Hourly averages of methane concentrations, showing seasonal variations. The color scheme is the following: Winter (black), Spring (green), Summer (red), Fall (yellow). Please note that, as stated above, the graph is referred to 2019 data only.

Table 2. The hourly values plotted in Figure 4 are listed, with the addition of standard deviations for each seasonal parameter. The table refers specifically to 2019.

Hours	Winter	Win. SD	Spring	Spr. SD	Summer	Sum. SD	Fall	Fa. SD
0	2076,27	163,49	2030,78	99,30	2066,69	113,04	2043,76	86,57
1	2076,78	157,14	2036,03	110,72	2078,96	118,00	2065,42	138,91
2	2087,11	162,39	2054,75	136,81	2084,67	124,21	2069,45	107,13
3	2082,18	161,63	2057,92	152,80	2102,78	130,50	2078,47	116,90
4	2087,75	174,86	2054,98	154,43	2088,88	123,60	2091,81	141,44
5	2079,08	156,14	2070,65	150,94	2086,37	122,84	2100,68	143,55
6	2089,18	167,36	2043,86	115,58	2045,54	100,81	2080,75	121,62
7	2096,24	178,82	2002,39	91,74	1980,23	57,72	2058,33	105,30
8	2043,12	120,53	1966,65	48,25	1943,77	26,59	1997,36	57,00
9	1994,23	90,90	1953,08	24,33	1933,72	16,59	1961,31	34,57
10	1964,34	38,20	1948,24	15,71	1931,18	14,27	1950,67	25,13
11	1955,17	27,22	1947,67	15,55	1929,20	14,54	1945,88	27,87
12	1953,52	24,69	1947,42	15,17	1926,67	13,62	1943,12	19,89
13	1952,92	25,71	1945,74	13,58	1925,17	14,20	1941,48	17,17
14	1951,27	17,15	1944,92	13,12	1925,21	15,02	1940,85	17,86
15	1952,23	18,01	1946,33	14,14	1924,65	14,22	1941,62	16,52
16	1956,75	24,34	1946,45	15,31	1924,85	14,36	1945,54	21,89
17	1967,86	38,03	1947,92	16,32	1926,58	19,07	1961,88	45,35
18	1979,94	49,42	1951,55	19,72	1928,99	31,05	1985,03	71,06
19	1994,36	65,39	1970,26	41,22	1938,43	40,10	1994,08	62,93
20	2009,53	83,48	1985,83	60,23	1977,44	92,46	2006,87	76,47

Preprints.org (www.preprints.org) | NOT PEER-REVIEWED | Posted: 19 July 2024 doi:10.20944/preprints202407.1587.v1

21	2030,08	102,69	2003,80	80,21	2019,90	111,61	2022,63	82,51
22	2046,53	124,62	2024,07	94,40	2033,38	115,17	2024,07	85,05
23	2051,48	135,37	2023,57	87,10	2051,06	114,79	2042,95	95,66

Overall, a prominent daily cycle is reported in Figure 4. Seasonal differences can also be noticed, with the Winter and Summer seasons yielding the highest and lowest values respectively, though this doesn't occur throughout the entire observation period. The "flat valley" in both absolute methane concentrations and hourly standard deviations occurring between 10:00 and 16:00 UTC is no coincidence, as the influence of local wind circulation on observed concentrations is known to be substantial. Identical graphs and tables, though applied to the other years, are accessible as Supplementary Material S1-A through S1-G. Graphs showing the variations in standard deviations are also accessible from these materials.

4.3. Chemical-Meteorological Evaluation

Pollution roses referred to 2019 are shown in Figure 5, grouped by season. For these evaluations, the secondary dataset described in Table 1 was used. As reported in section 2, the observation site is affected by two distinct wind circulation corridors: a pure western-seaside sector yielding generally lower methane concentrations, and a northeastern-continental sector showing much higher concentrations. Pollution roses reporting data referred to the other years are accessible as Supplementary Material S2-A through S2-F.

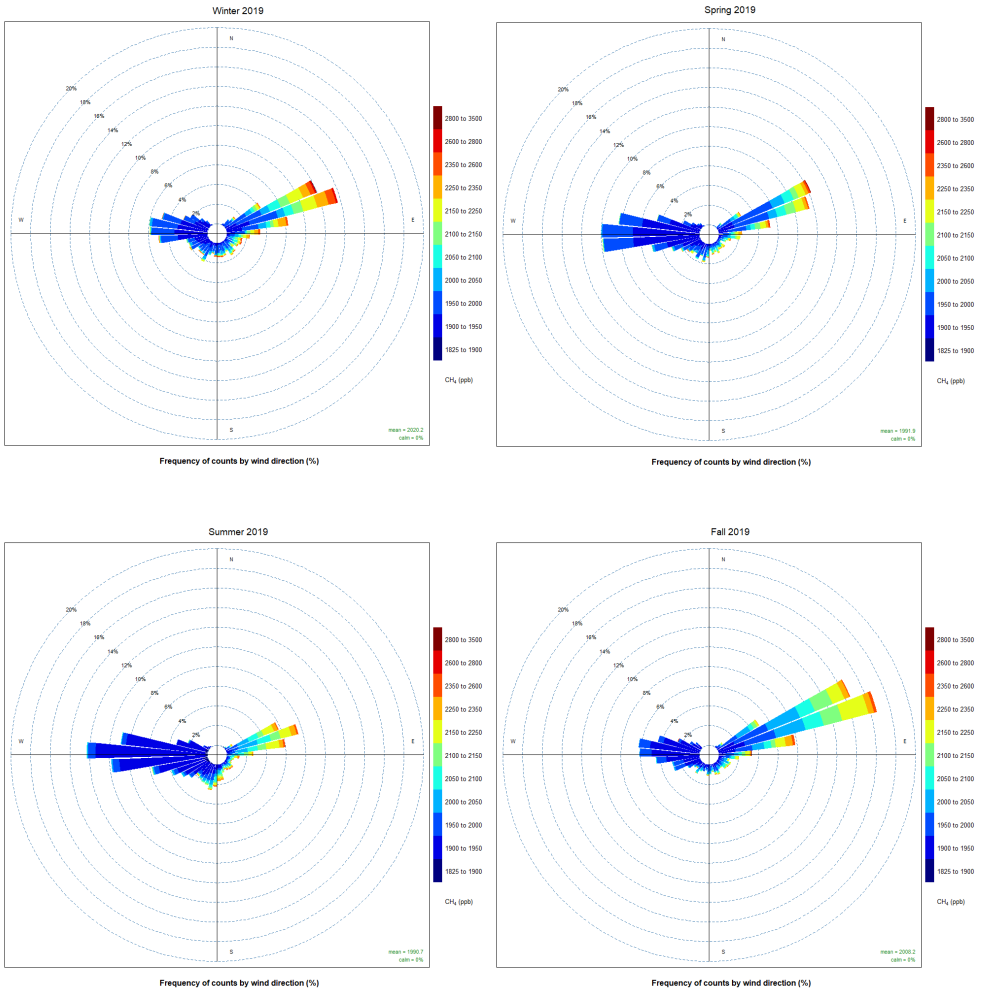

Figure 5. Seasonal pollution roses of methane concentrations observed at LMT referred to 2019. Each bar represents an angle of 8 degrees.

 doi:10.20944/preprints202407.1587.v1

Via the application of two distinct filters, observed methane concentrations have been correlated with wind speeds. In particular, a western-seaside sector (240-300 °N, 3260 hours) and a northeastern-continental (0-90 °N, 2921 hours) sector have been filtered from the secondary dataset, constituting respectively 38,13% and 34,17% of 2019's available data. 27,7% of detections fall outside these ranges. The results are shown in Figure 6 and clearly indicate how the highest methane concentrations are linked to northeastern winds, in conjunction with lower wind speeds (Figure 6B). Winds coming from the west sector yield considerably lower methane concentrations, even though wind speeds are variable and winter-time peaks exceeding 14m/s can be noticed (Figure 6A). Also, note how – if combined – the two sectors would lean to a hyperbola branch distribution, as shown in Supplementary Material S3-G (the supplementary graph also includes values falling outside the two ranges). Supplementary Material S3-A through S3-F shows the same graphs applied to years other than 2019, while S3-G shows all observed values.

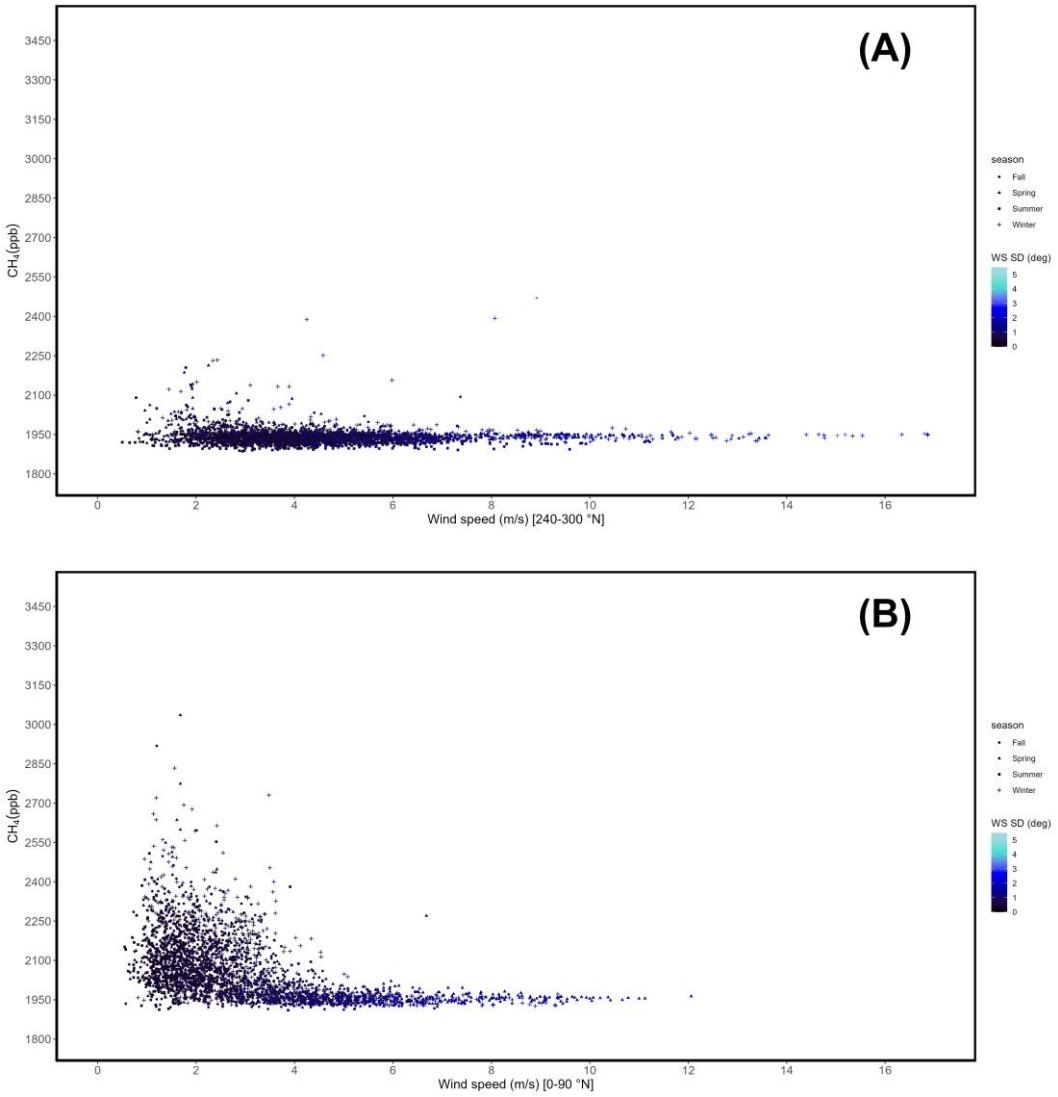

Figure 6. Correlations between observed wind speeds (X axis) and methane concentrations (Y axis). A: Western-seaside sector (240-300 °N). B: Northeastern-continental sector (0-90 °N). The color scheme is set to represent hourly changes in wind speed standard deviations.

4.4. Outbreak Analysis

A further evaluation was aimed specifically at possible indicators of anthropic activities, which could be susceptible to weekdays, under the assumption that no natural mechanism would lead to substantial statistical differences affecting the occurrence of outbreak events during a week. In the

 doi:10.20944/preprints202407.1587.v1

case of 2019, two distinct evaluations have been performed on a per-weekday basis, one accounting for values equal or greater than the 3rd quartile (2029,11 ppb), and a second, more constrained evaluation accounting for the top 2,5% values (2299,91 ppb). The analysis was performed on the primary Picarro G2401 dataset. Respectively, 2138 and 214 hours satisfied these conditions, now plotted in Figure 7. Supplementary Material S4-A through S4-F shows results concerning years other than 2019. Table 3 shows the two filters, including the number of hours satisfying their conditions, throughout the entire 2016-2022 period.

Table 3. 3rd quartile and 97,5% threshold counts data and details, per year. The last row shows the total number of hours exceeding the two limits, as well as the average count of hours satisfying that condition, by weekday.

Year	3rd Q. (ppb)	Hours ≥ 3rd Q.	Average count per weekday (3rd Q.)	97,5% threshold (ppb)	Hours ≥ 97,5% threshold	Average count per weekday (97,5%)
2016	1994,2	2085	297,85	2418,76	209	29,85
2017	2031,23	2181	311,57	2401,73	219	31,28
2018	2017,44	2059	294,14	2346,05	206	29,42
2019	2029,11	2138	305,71	2299,91	214	30,57
2020	2056,46	2060	294,28	2278,84	206	29,42
2021	2069,5	2140	305,71	2337,82	214	30,57
2022	2117,58	1836	262,28	2432,91	184	26,28
		14499[1]	2071,28[2]		1452[1]	207,42[2]

[1] Total amount. [2] Average value.

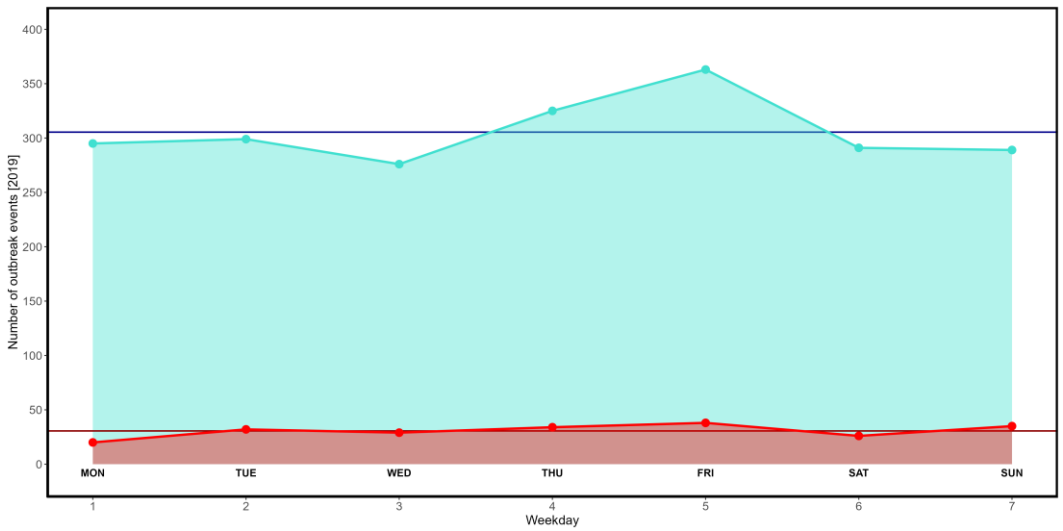

Figure 7. Weekly (MON-SUN) distribution of outbreak events exceeding the 3rd quartile (turquoise) and 97,5% threshold (red) in 2019. The two y axis intercepts show the average number of outbreak events per weekday, which is 305,71 and 30,57 respectively.

A Chi-squared test was performed on combined data concerning outbreak events listed by weekday. Said test was executed in R 4.4.0 by setting a value of 9999 Monte Carlo replicates. Table 4 reports the data used, as well as the computed χ^2 and p-values. For the graph, see Supplementary Material S4-G. Though over the course of the observation period a variability in peaks per weekday can be noticed (see Supplementary Material S4-A through S4-F), combined 2016-2022 data points to Friday as the day with the most frequent occurrence of outbreaks. The 3rd quartile category has provided a more statistically relevant result in terms of distribution.

Table 4. Results of the Chi-squared test performed to verify the possible outbreak occurrence susceptibility to specific weekdays. For the graph, see Supplementary Material S4-G.

 doi:10.20944/preprints202407.1587.v1

Type	Average	MON	TUE	WED	THU	FRI	SAT	SUN	χ^2	*p*-value
3rd Q.	2071,28	1899	2024	2089	2163	2246	2082	1996	37,152	0,0001
97,5% th.	207,42	181	179	210	201	251	207	223	17,817	0,0064

4.5. Multi-Year Trend

Finally, a multiyear trend has been plotted with the integration of a regression line and equation meant to fit observed variations over time. The observed increasing trend is statistically significant. For this evaluation, the year 2022 has been excluded due to its lower coverage rate of 83,83% compared to the other years, which fall in the 93,8-99,57% range (see Table 1). Figure 8 also shows a regression equation based on this data, which yields a result of:

$$y\ (CH_4, ppb) = 10 \times (year) + 19000 \qquad R = 0.93,\ R^2_{adj} = 0.84,\ p = 0.0067 \quad \text{(Eq. 1)}$$

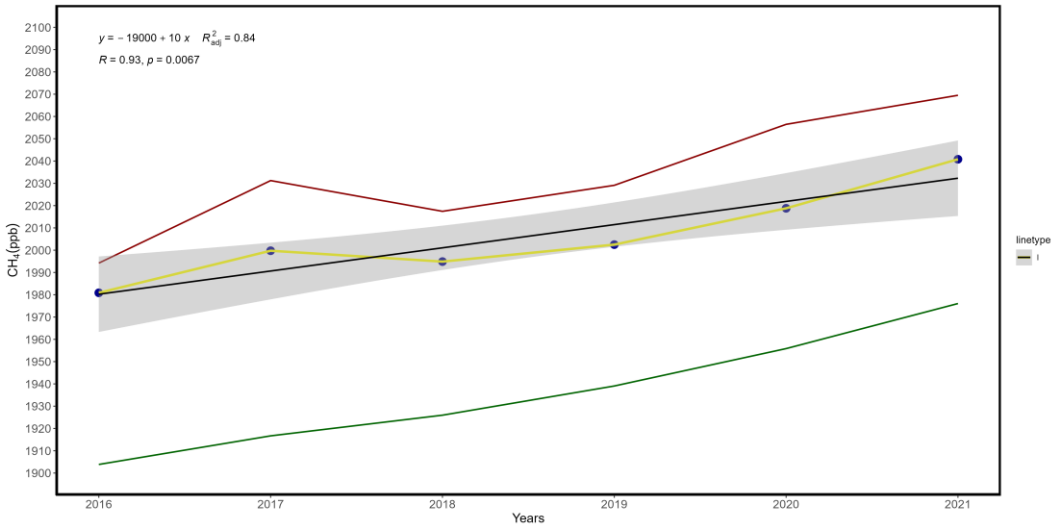

Figure 8. Average annual methane values over the course of LMT's observation history, except for 2022 due to its lower coverage rate compared to 2016-2021 (see Tables 1, 5). Also included are annual trends in 3rd quartile (dark red) and 1st quartile (dark green) values.

Table 5. Annual means of methane concentrations and their respective standard deviations, in ppb. The year 2022, written in italic, is excluded from Figs. 7 and 8. NOAA annual means and changes are extrapolated from Lan et al. (2024) [34].

Year	CH4 (ppb)	CH4 SD (ppb)	Coverage (%)	Change (ppb)	NOAA (ppb)	NOAA change (ppb)	LMT-NOAA diff. (ppb)
2016	1980,87	146,78	94,92	-	1843,12	+7,05	137,75
2017	1999,75	140,30	99,57	+18,88	1849,67	+6,89	150,08
2018	1994,88	121,38	94	-4,87	1857,33	+8,70	137,55
2019	2002,50	106,98	97,6	+7,62	1866,58	+9,67	135,92
2020	2018,79	96,20	93,8	+16,29	1878,93	+15,17	139,86
2021	2040,79	105,99	97,71	+22,00	1895,28	+17,91	145,51
2022[1]	*2074,87*	*126,87*	*83,83*	*+34,07*	*1922,53*	*+13,26*	*137,75*

[1] 2022 is reported in italics but not featured in Figs. 8, 9.

The global annual means issued by NOAA and LMT's observations have been compared. Differences between annual means are shown in Table 5. Overall, with the exception of a surge in 2017 (difference: 150,08 ppb), five annual differences in the 2016-2021 period fall in the 135,92-139,86 ppb range, with the 2022 divergence being identical to that of 2016. Both trends are shown in Figure 9.

 doi:10.20944/preprints202407.1587.v1

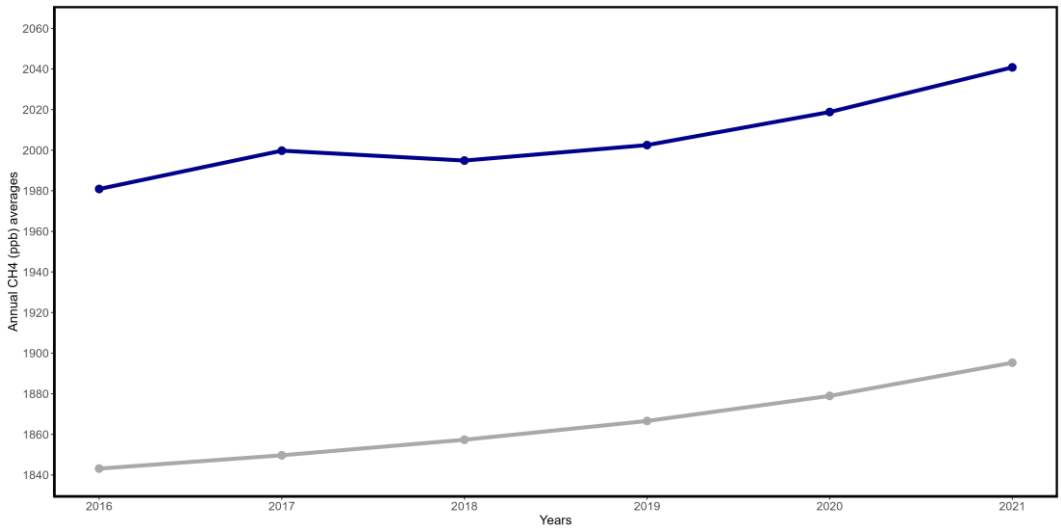

Figure 9. Direct comparison of LMT (dark blue) and global NOAA (dark gray) annual means.

Both Table 5 and Figure 9 remark 2020 surges which are likely related to the Covid-19 pandemic, which is known to have led to an increase in global CH_4 concentrations [34,35]. On average, LMT annual means exceed the global NOAA values by 141,11 ppb. The 2017 surge is local.

5. Discussion

The larger data set and the integration of key meteorological information have allowed a more detailed analysis on methane concentrations detected at the LMT observatory. The detailed analysis on methane detections from the 0-90 °N range allows to better constrain some of the hypotheses made in the past on local sources of pollution. Research such as Cristofanelli et al. (2017) [28] proposed local livestock farming, air traffic, and landfills among the causes of higher levels, and that is compatible with the observed wind directions, as the location of at least one local farm, as well as that of a landfill, are indeed compatible with these wind trajectories and their methane peaks.

The general trend seen in Figure 3 highlights seasonal cycles and an upward trend towards higher concentrations over time, while the daily cycles seen in Figure 4 are dominated by wind circulation. “Flat valleys” in hourly graphs are linked to western winds. The further analysis of methane concentrations with respect to wind directions (Figure 5) and speed (Figure 6) has allowed to determine the existence of two main corridors: a western-seaside direction, linked to lower methane concentrations regardless of wind speed, and a northeastern-continental direction, which is characterized by higher methane mole fractions (especially in the case of low wind speeds), which are likely due to nearby sources of this compound. The corridors are susceptible to seasonal variations, as reported in Figure 5 and related supplementary materials.

For the first time in the data gathering history of the observation site LMT a possible correlation between weekdays and outbreak events was tested under the assumption that no mechanism in nature other than anthropic would lead to statistically significant differences in outbreak event occurrence over the course of weekdays. Figure 7 and Table 4, as well as related Supplementary Material 4-A through 4-G, provide statistical relevance to higher results on Fridays, though it’s worth noting that each year’s results show several degrees of variability. Friday peaks may be the result of commuting, public transportation, farming and industrial activities, though future works will have to investigate these occurrences even further. The fact that both Mondays and Sundays yield lower averages also seems to point in the direction of a hypothetical “weekly” cycle, likely affected by anthropic activities.

Overall, the results shown in this work with respect to methane concentration variability depending on wind direction, combined with the statistical distribution of outbreaks over the course of weekdays, seem to corroborate the hypothesis seen in previous studies such as Cristofanelli et al.

 doi:10.20944/preprints202407.1587.v1

(2017) [28] by which anthropic sources located in the northeast with respect to LMT are responsible for generally higher methane concentrations in the area. In the context of a "multisource" scenario, the previous study reported in particular two possible sources of methane in the area: local livestock farming, and air traffic.

Livestock such as cattle are indeed responsible for major methane emissions levels worldwide [36,37] and contribute up to an estimated 14,5% of total anthropogenic greenhouse gas emissions. Specifically, Hristov et al. (2013) [38] reported that each cow releases 60-160 kg CH_4 y^{-1} while goats and sheep release 10-16 kg CH_4 y^{-1}, all depending on characteristics such as the dry matter intake parameter (DMI) and size of the ruminant. In the case of observed methane concentrations at LMT, it is currently impossible to pinpoint emissions strictly related to livestock farming in the area unless new parameters such as carbon isotope fractionation are considered.

Similarly, the influence of local air traffic is also difficult to estimate, and for a number of reasons, including operational characteristics and aeronautical procedures. One preliminary conclusion would be that the observatory and the airport's runways intersect two parallel air corridors which don't affect each other, but the leading literature on air traffic pollution and emissions place the LMT station inside the "near-airport" (<10km) range category, which is – according to studies such as Carslaw et al. (2006) [36] and Carslaw & Beevers, (2013) [37] – subject to direct air traffic influence. Aircraft engine combustion processes are among known sources of methane and do contribute to anthropic climate change [41,42]. Literature on air quality perturbation by air traffic has also focused on LTO (Landing to Take-Off) cycles, which are related to operational phases during which aircraft are either on ground or at low altitudes [43,44], while research on broader effects of air traffic also considers cruise phases [45,46]. The airport was recognized in previous research as a possible influence over LMT's detections [28], but no source apportionment has been performed. Specifically, runway (RWY) 10 take-offs (aircraft facing east) and RWY 28 landings (aircraft facing west) would place aircraft on trajectories compatible with the northeastern-continental wind sector shown in Figure 5 and related supplementary material. It is presently not possible, without the introduction of additional tracers, to provide tangible estimates concerning the airport's influence over local methane detections.

Finally, relevant assumptions can be made when considering multi-year trends observed at LMT. Globally, methane concentrations are on the rise as a result of anthropic activities, but on a local scale – though the clear upward trend persists – sporadic "bursts" of concentrations may occur, such as the 2017 peak reported in Figure 8, 9 and Table 5. In 2020, a year heavily affected by the Covid-19 pandemic, global values experienced a 15 ppb increase [13,34] which is similar to the 16,29 ppb surge observed at Lamezia Terme's observatory. It's worth noting that an annual global increase of 1 ppb is believed to be the result of extra ≈ 2.77 Tg CH_4 being emitted into the atmosphere [5]. The 2019-2020 local-to-global leap is no surprise, as the Covid-19 outbreak lockdowns have caused an unexpected increase in methane concentrations [35]. Methane has a latency of approximately one decade in the atmosphere, but several models clearly show that the peak response of this alkane occurs within a few months from extra-emission pulses [47,48], corroborating the hypothesis by which the 2020 peak is linked to nation-wide lockdowns and consequent increases in emissions from the energy sector [49], though the 2020 peak is likely due to a combination of multiple factors. A recent study by Feng et al. (2023) [50] estimated that 66% of the 2020 methane surge was due to increased emission rates.

6. Conclusions

For the first time, multi-year trends of methane detected by the Lamezia Terme WMO/GAW station (LMT) have been analyzed. Located close to the Tyrrhenian coast of Calabria, in the narrowest point of the Italian peninsula, measurements at this observatory are largely influenced by its peculiar location in the country. Daily cycles are influenced by local wind circulation and synoptic: a western-seaside sector yields lower methane concentrations, while northeastern-continental winds yield the highest concentrations detected at LMT. The circulation is such that daytime winds come mostly from the western sector, thus resulting in much lower methane values, while nocturnal winds come from

 doi:10.20944/preprints202407.1587.v1

the northeast. Filtering data by wind direction clearly demonstrates the differences in terms of average concentrations as detected from the two sectors. Moreover, wind speed is also very closely tied to methane values, as the comparison of methane concentrations and wind speeds results into a hyperbola branch pattern where low speeds are linked to higher values and, vice versa, high speeds yielded lower values. Seasonal differences and cycles are also well-defined, with Winter and Summer seasons generally yielding the highest and lowest methane concentrations, respectively. Multi-year trends have been compared with NOAA's global measurements: the trends are similar and differences between yearly averages fall mostly within a well-defined window, though it's worth noting that methane concentrations are known from literature to vary depending on geographical factors such as latitude. A local surge in 2017 is reported and results into the highest observed divergence between yearly LMT and NOAA data. Overall, the results presented by this study confirm an upward trend in methane, which is a potent greenhouse gas. For the first time, a method was introduced to correlate outbreak events of methane concentrations with weekdays in the effort to determine possible anthropic influences over these values, as anthropic activities alone do have a weekly cycle which is totally lacking in nature. The results indicate that peaks tend to occur on Fridays, while Mondays and Sundays yielded lower values. The introduction of $\delta^{13}C$ measurements of CH_4, as well as CO_2, would significantly help with source apportionment in future studies.

Supplementary Materials: The following supporting information can be downloaded at the website of this paper posted on Preprints.org, *[see dedicated section below for peer reviewing purposes]*.

Author Contributions: Conceptualization, F.D. and C.R.C.; methodology, F.D., C.R.C. and T.L.F.; software, F.D.; validation, C.R.C., T.L.F. and P.C.; formal analysis, F.D.; investigation, F.D.; data curation, F.D., I.A., D.G., E.A., T.L.F., P.C., L.M., D.P., S.S. and G.D.B.; writing—original draft preparation, F.D.; writing—review and editing, F.D., CR.R., I.A., D.G., E.A., T.L.F., M.D.P., P.C., L.M., D.P., S.S. and G.D.B.; visualization, F.D., C.R.C., D.G. and T.L.F.; supervision, C.R.C. and P.C.; funding acquisition, C.R.C. and M.D.P. All authors have read and agreed to the published version of the manuscript.

Funding: This research was funded by AIR0000032 – ITINERIS, the Italian Integrated Environmental Research Infrastructures System (D.D. n. 130/2022 - CUP B53C22002150006) under the EU - Next Generation EU PNRR - Mission 4 "Education and Research" - Component 2: "From research to business" - Investment 3.1: "Fund for the realization of an integrated system of research and innovation infrastructures".

Data Availability Statement: The datasets presented in this article are not readily available because they are part of other ongoing studies.

Acknowledgments: To be filled in later (anonymous reviewers, editors).

Conflicts of Interest: The authors declare no conflicts of interest.

References

1. Byrom, R.E.; Shine, K.P. Methane's Solar Radiative Forcing. *Geophys. Res. Lett.* **2022**, *49(15)*, e2022GL098270. https://doi.org/10.1029/2022GL098270.
2. Myhre, G.; Shindell, D.; Bréon, F.M.; Collins, W.; Fuglestvedt, J.; Huang, J.; Koch, D.; Lamarque, J.F.; Lee, D.; Mendoza, B.; Nakajima, T.; Robock, A.; Stephens, G.; Takemura, T.; Zhan, H. Anthropogenic and Natural Radiative Forcing. In *Climate Change 2013: The Physical Science Basis, Contribution of Working Group I to the Fifth Assessment Report of the Intergovernmental Panel on Climate Change*. Cambridge, UK and New York, 2013.
3. Sand, M.; Skeie, R.B.; Sandstad, M.; Krishnan, S.; Myhre, G.; Bryant, H.; Derwent, R.; Hauglustaine, D.; Paulot, F.; Prather, M.; Stevenson, D. A multi-model assessment of the Global Warming Potential of hydrogen. *Nat. Commun.* **2023**, *4*, 203. https://doi.org/10.1038/s43247-023-00857-8.
4. Etheridge, D.M.; Steele, L.P.; Francey, R.J.; Langenfelds, R.L. Atmospheric methane between 1000 A.D. and present: Evidence of anthropogenic emissions and climatic variability. *J. Geophys. Res. Atmospheres* **1998**, *103*, pgs. 15979–15993. https://doi.org/10.1029/98jd00923.
5. Nisbet, E.G.; Manning, M.R.; Dlugokencky, E.J.; Fisher, R.E.; Lowry, D.; Michel, S.E.; Lund Myhre, C.; Platt, S.M.; Allen, G.; Bousquet, P.; Brownlow, R.; Cain, M.; France, J.L.; Hermansen, O.; Hossaini, R.; Jones, A.E.; Levin, I.; Manning, A.C.; Myhre, G.; Pyle, J.A.; Vaughn, B.H.; Warwick, N.J.; White, J.W.C. Very Strong Atmospheric Methane Growth in the 4 Years 2014–2017: Implications for the Paris Agreement. *Global Biogeochem. Cycles* **2019**, *33(3)*, pgs. 318-342. https://doi.org/10.1029/2018GB006009.

6. Blunden, J.; Boyer, T.; Bartow-Gillies, E. State of the Climate in 2022. *B. Am. Meteorol. Soc.* **2023**, *104(9)*, pgs. 1–501. https://doi.org/10.1175/2023BAMSStateoftheClimate.1.
7. Skeie, R.B.; Hodnebrog, Ø.; Myhre, G. Trends in atmospheric methane concentrations since 1990 were driven and modified by anthropogenic emissions. *Commun. Earth Environ.* **2023**, *4*, 317. https://doi.org/10.1038/s43247-023-00969-1.
8. Szopa, S.; Naik, V.; Adhikary, B.; Artaxo, P.; Berntsen, T.; Collins, W.D.; Fuzzi, S.; Gallardo, L.; Kiendler-Scharr, A.; Klimont, Z.; Liao, H.; Unger, N.; Zanis, P. Short-Lived Climate Forcers. In: *Climate Change 2021: The Physical Science Basis. Contribution of Working Group I to the Sixth Assessment Report of the Intergovernmental Panel on Climate Change*, edited by: Masson-Delmotte, V., Zhai, P., Pirani, A., Connors, S.L., Péan, C., Berger, S., Caud, N., Chen,Y., Goldfarb, L., Gomis, M.I., Huang, M., Leitzell, K., Lonnoy, E., Matthews, J.B.R., Maycock, T.K., Waterfield, T., Yelekçi, O., Yu, R., and Zhou, B. Cambridge University Press, Cambridge, United Kingdom and New York, NY, USA, 2021, pgs. 817–922.
9. Dlugokencky, E.J.; Steele, L.P.; Lang, P.M.; Masarie, K.A. The growth rate and distribution of atmospheric methane. *J. Geophys. Res. Atmospheres* **1994**, *99*, D8, pgs. 17021-17043. https://doi.org/10.1029/94JD01245.
10. Saunois, M.; Bousquet, P.; Poulter, B.; Peregon, A.; Ciais, P.; Canadell, J.G.; Dlugokencky, E. J.; Etiope, G.; Bastviken, D.; Houweling, S.; Janssens-Maenhout, G.; Tubiello, F.N.; Castaldi, S.; Jackson, R.B.; Alexe, M.; Arora, V.K.; Beerling, D.J.; Bergamaschi, P.; Blake, D.R.; Brailsford, G.; Brovkin, V.; Bruhwiler, L.; Crevoisier, C.; Crill, P.; Covey, K.; Curry, C.; Frankenberg, C.; Gedney, N.; Höglund-Isaksson, L.; Ishizawa, M.; Ito, A.; Joos, F.; Kim, H.-S.; Kleinen, T.; Krummel, P.; Lamarque, J.-F.; Langenfelds, R.; Locatelli, R.; Machida, T.; Maksyutov, S.; McDonald, K.C.; Marshall, J.; Melton, J.R.; Morino, I.; Naik, V.; O'Doherty, S.; Parmentier, F.-J.W.; Patra, P.K.; Peng, C.; Peng, S.; Peters, G.P.; Pison, I.; Prigent, C.; Prinn, R.; Ramonet, M.; Riley, W.J.; Saito, M.; Santini, M.; Schroeder, R.; Simpson, I.J.; Spahni, R.; Steele, P.; Takizawa, A.; Thornton, B.F.; Tian, H.; Tohjima, Y.; Viovy, N.; Voulgarakis, A.; van Weele, M.; van der Werf, G.R.; Weiss, R.; Wiedinmyer, C.; Wilton, D.J.; Wiltshire, A.; Worthy, D.; Wunch, D.; Xu, X.; Yoshida, Y.; Zhang, B.; Zhang, Z.; Zhu, Q. The global methane budget 2000–2012. *Earth Syst. Sci. Data* **2016**, *8*, pgs. 697–751. https://doi.org/10.5194/essd-8-697-2016.
11. Saunois, M.; Bousquet, P.; Poulter, B.; Peregon, A.; Ciais, P.; Canadell, J.G.; Dlugokencky, E.J.; Etiope, G.; Bastviken, D.; Houweling, S.; Janssens-Maenhout, G.; Tubiello, F.N.; Castaldi, S.; Jackson, R.B.; Alexe, M.; Arora, V.K.; Beerling, D.J.; Bergamaschi, P.; Blake, D.R.; Brailsford, G.; Bruhwiler, L.; Crevoisier, C.; Crill, P.; Covey, K.; Frankenberg, C.; Gedney, N.; Höglund-Isaksson, L.; Ishizawa, M.; Ito, A.; Joos, F.; Kim, H.-S.; Kleinen, T.; Krummel, P.; Lamarque, J.-F.; Langenfelds, R.; Locatelli, R.; Machida, T.; Maksyutov, S.; Melton, J.R.; Morino, I.; Naik, V.; O'Doherty, S.; Parmentier, F.-J.W.; Patra, P.K.; Peng, C.; Peng, S.; Peters, G.P.; Pison, I.; Prinn, R.; Ramonet, M.; Riley, W.J.; Saito, M.; Santini, M.; Schroeder, R.; Simpson, I.J.; Spahni, R.; Takizawa, A.; Thornton, B.F.; Tian, H.; Tohjima, Y.; Viovy, N.; Voulgarakis, A.; Weiss, R.; Wilton, D.J.; Wiltshire, A.; Worthy, D.; Wunch, D.; Xu, X.; Yoshida, Y.; Zhang, B.; Zhang, Z.; Zhu, Q. Variability and quasi-decadal changes in the methane budget over the period 2000–2012. *Atmos. Chem. Phys.* **2017**, *17*, pgs. 11135–11161. https://doi.org/10.5194/acp-17-11135-2017.
12. Saunois, M.; Stavert, A.R.; Poulter, B.; Bousquet, P.; Canadell, J.G.; Jackson, R.B.; Raymond, P.A.; Dlugokencky, E.J.; Houweling, S.; Patra, P.K.; Ciais, P.; Arora, V.K.; Bastviken, D.; Bergamaschi, P.; Blake, D.R.; Brailsford, G.; Bruhwiler, L.; Carlson, K.M.; Carrol, M.; Castaldi, S.; Chandra, N.; Crevoisier, C.; Crill, P.M.; Covey, K.; Curry, C.L.; Etiope, G.; Frankenberg, C.; Gedney, N.; Hegglin, M.I.; Höglund-Isaksson, L.; Hugelius, G.; Ishizawa, M.; Ito, A.; Janssens-Maenhout, G.; Jensen, K.M.; Joos, F.; Kleinen, T.; Krummel, P.B.; Langenfelds, R.L.; Laruelle, G.G.; Liu, L.; Machida, T.; Maksyutov, S.; McDonald, K.C.; McNorton, J.; Miller, P.A.; Melton, J.R.; Morino, I.; Müller, J.; Murguia-Flores, F.; Naik, V.; Niwa, Y.; Noce, S.; O'Doherty, S.; Parker, R.J.; Peng, C.; Peng, S.; Peters, G.P.; Prigent, C.; Prinn, R.; Ramonet, M.; Regnier, P.; Riley, W.J.; Rosentreter, J.A.; Segers, A.; Simpson, I.J.; Shi, H.; Smith, S.J.; Steele, L.P.; Thornton, B.F.; Tian, H.; Tohjima, Y.; Tubiello, F.N.; Tsuruta, A.; Viovy, N.; Voulgarakis, A.; Weber, T.S.; van Weele, M.; van der Werf, G.R.; Weiss, R.F.; Worthy, D.; Wunch, D.; Yin, Y.; Yoshida, Y.; Zhang, W.; Zhang, Z.; Zhao, Y.; Zheng, B.; Zhu, Q.; Zhu, Q.; Zhuang, Q. The Global Methane Budget 2000–2017. *Earth Syst. Sci. Data* **2020**, *12*, pgs. 1561–1623. https://doi.org/10.5194/essd-12-1561-2020.
13. Lan, X.; Nisbet, E.G.; Dlugokencky, E.J.; Michel, S.E. What do we know about the global methane budget? Results from four decades of atmospheric CH_4 observations and the way forward. *Philos. Trans. A Math. Phys. Eng. Sci.* **2021**, *379*, 20200440. https://doi.org/10.1098/rsta.2020.0440.
14. IEA Methane Tracker 2021. International Energy Agency, Paris, 2021. Source: https://www.iea.org/reports/methane-tracker-2021.
15. Etiope, G.; Ciotoli, G.; Schwietzke, S.; Schoell, M. Gridded maps of geological methane emissions and their isotopic signature. *Earth Syst. Sci. Data* **2019**, *11*, pgs. 1–22. http://dx.doi.org/10.5194/essd-11-1-2019.
16. Chang, J.; Peng, S.; Ciais, P.; Saunois, M.; Dangal, S.R.S.; Herrero, M.; Havlík, P.; Tian, H.; Bousquet, P. Revisiting enteric methane emissions from domestic ruminants and their $\delta^{13}C_{CH4}$ source signature. *Nat. Commun.* **2019**, *10*, 3420. https://doi.org/10.1038/s41467-019-11066-3.

17. Dlugokencky, E.; Nisbet, E.G.; Fisher, R.; Lowry, D. Global atmospheric methane: budget, changes and dangers. *Philos. Trans. A Math. Phys. Eng. Sci.* **2011**, *369(1943)*. https://doi.org/10.1098/rsta.2010.0341.
18. Blake, D.R.; Mayer, E.W.; Tyler, S.C.; Makide, Y.; Montague, D.C.; Rowland, F.S. Global increase in atmospheric methane concentrations between 1978 and 1980. *Geophys. Res. Lett.* **1982**, *9*, pgs. 477–480. http://dx.doi.org/10.1029/GL009i004p00477.
19. Yu, L.; Huang, Y.; Zhang, W.; Li, T.; Sun, W. Methane uptake in global forest and grassland soils from 1981 to 2010. *Sci. Total Environ.* **2017** *607-608*, pgs. 1163-1172. https://doi.org/10.1016/j.scitotenv.2017.07.082.
20. Pison, I.; Ringeval, B.; Bousquet, P.; Prigent, C.; Papa, F. Stable atmospheric methane in the 2000s: key-role of emissions from natural wetlands. *Atmos. Chem. Phys.* **2013** *13*, pgs. 11609–11623. https://www.doi.org/10.5194/acp-13-11609-2013.
21. Dlugokencky, E.; Masarie, K.; Lang, P.; Tans, P.P. Continuing decline in the growth rate of the atmospheric methane burden. *Nature* **1998**, *393*, pgs. 447–450. http://dx.doi.org/10.1038/30934.
22. Dlugokencky, E.J.; Houweling, S.; Bruhwiler, L.; Masarie, K.A.; Lang, P.M.; Miller, J.B.; Tans, P.P. Atmospheric methane levels off: Temporary pause or a new steady-state? *Geophys. Res. Lett* **2003**, *30(19)*. https://doi.org/10.1029/2003GL018126.
23. He, J.; Naik, V.; Horowitz, L.W.; Dlugokencky, E.; Thoning, K. Investigation of the global methane budget over 1980–2017 using GFDL-AM4.1. *Atmos. Chem. Phys.* **2020**, *20*, pgs. 805–827. https://doi.org/10.5194/acp-20-805-2020.
24. Ferretti, D.F.; Miller, J.B.; White, J.W.C.; Etheridge, D.M.; Lassey, K.R.; Lowe, D.C.; Macfarling Meure, C.M.; Dreier, M.F.; Trudinger, C.M.; Van Ommen, T.D.; Langenfelds, R.L. Unexpected changes to the global methane budget over the past 2000 years. *Science* **2005**, *309(5741)*, pgs. 1714–1717. https://doi.org/10.1126/science.1115193.
25. Peng, S.; Lin, X.; Thompson, R.L.; Xi, Y.; Liu, G.; Hauglustaine, D.; Lan, X.; Poulter, B.; Ramonet, M.; Saunois, M.; Yin, Y.; Zhang, Z.; Zheng, B.; Ciais, P. Wetland emission and atmospheric sink changes explain methane growth in 2020. *Nature* **2022**, *612*, pgs. 477–482. https://doi.org/10.1038/s41586-022-05447-w.
26. Wilson, C. Untangling variations in the global methane budget. *Nat. Commun.* **2023** *4*, 318. https://doi.org/10.1038/s43247-023-00971-7.
27. Federico, S.; Pasqualoni, L.; De Leo, L.; Bellecci, C. A study of the breeze circulation during summer and fall 2008 in Calabria, Italy. *Atmos. Res.* **2010**, *97(1-2)*, pgs. 1-13. https://doi.org/10.1016/j.atmosres.2010.02.009.
28. Cristofanelli, P.; Busetto, M.; Calzolari, F.; Ammoscato, I.; Gullì, D.; Dinoi, A.; Calidonna, C.R.; Contini, D.; Sferlazzo, D.; Di Iorio, T.; Piacentino, S.; Marinoni, A.; Maione, M.; Bonasoni, P. Investigation of reactive gases and methane variability in the coastal boundary layer of the central Mediterranean basin. *Elem. Sci. Anth.* **2017** *5, 12*. https://doi.org/10.1525/elementa.216.
29. Federico, S.; Pasqualoni, L.; Sempreviva, A.M.; De Leo, L.; Avolio, E.; Calidonna, C.R.; Bellecci, C. The seasonal characteristics of the breeze circulation at a coastal Mediterranean site in South Italy. *Adv. Sci. Res.* **2010**, *4*, pgs. 47–56. https://doi.org/10.5194/asr-4-47-2010.
30. Gullì, D.; Avolio, E.; Calidonna, C.R.; Lo Feudo, T.; Torcasio, R.C.; Sempreviva, A.M. Two years of wind-lidar measurements at an Italian Mediterranean Coastal Site. In European Geosciences Union General Assembly 2017, EGU – Division Energy, Resources & Environment, ERE. *Energy Procedia* **2017**, *125*, pgs. 214-220. https://doi.org/10.1016/j.egypro.2017.08.194.
31. Lo Feudo, T.; Calidonna, C.R.; Avolio, E.; Sempreviva, A.M. Study of the Vertical Structure of the Coastal Boundary Layer Integrating Surface Measurements and Ground-Based Remote Sensing. *Sensors* **2020**, *20*, 6516. https://doi.org/10.3390/s20226516.
32. Malacaria, L.; Parise, D.; Lo Feudo, T.; Avolio, E.; Ammoscato, I.; Gullì, D.; Sinopoli, S.; Cristofanelli, P.; De Pino, M.; D'Amico, F.; Calidonna, C.R. Multiparameter detection of summer open fire emissions: the case study of GAW regional observatory of Lamezia Terme (Southern Italy). *Fire* **2024**, *7(6)*, 198. https://doi.org/10.3390/fire7060198.
33. Calidonna, C.R.; Avolio, E.; Gullì, D.; Ammoscato, I.; De Pino, M.; Donateo, A.; Lo Feudo, T. Five Years of Dust Episodes at the Southern Italy GAW Regional Coastal Mediterranean Observatory: Multisensors and Modeling Analysis. *Atmosphere* **2020**, *11(5)*, 456. https://doi.org/10.3390/atmos11050456.
34. Lan, X.; Thoning, K.W.; Dlugokencky, E.J. Trends in globally-averaged CH_4, N_2O, and SF_6 determined from NOAA Global Monitoring Laboratory measurements. Version 2024-06, 2024. Available online: https://doi.org/10.15138/P8XG-AA10.
35. Laughner, J.L.; Neu, J.L.; Schimel, D.; Wennberg, P.O.; Barsanti, K.; Bowman, K.W.; Chatterjee, A.; Croes, B.E.; Fitzmaurice, H.L.; Henze, D.K.; Kim, J.; Kort, E.A.; Liu, Z.; Miyazaki, K.; Turner, A.J.; Anenberg, S.; Avise, J.; Cao, H.; Crisp, D.; de Gouw, J.; Eldering, A.; Fyfe, J.C.; Goldberg, D.L.; Gurney, K. R.; Hasheminassab, S.; Hopkins, F.; Ivey, C.E.; Jones, D.B.A.; Liu, J.; Lovenduski, N.S.; Martin, R.V.; McKinley, G.A.; Ott, L.; Poulter, B.; Ru, M.; Sander, S.P.; Swart, N.; Yung, Y.L.; Zeng, Z.-C. Societal shifts due to COVID-19 reveal large-scale complexities and feedbacks between atmospheric chemistry and climate change. *Proc. Natl. Acad. Sci.* **2021**, *118*, e2109481118. https://doi.org/10.1073/pnas.2109481118.

36. Grossi, G.; Goglio, P.; Vitali, A.; Williams, A.G. Livestock and climate change: impact of livestock on climate and mitigation strategies. *Animal Frontiers* **2019**, *9(1)*, pgs. 69-76. https://www.doi.org/10.1093/af/vfy034.
37. Tapio, I.; Snelling, T.J.; Strozzi, F.; Wallace, R.J. The ruminal microbiome associated with methane emissions from ruminant livestock. *J. Anim. Sci. Biotechnol.* **2017**, *8*, 7. https://doi.org/10.1186/s40104-017-0141-0.
38. Hristov, A.N.; Oh, J.; Firkins, J.L.; Dijkstra, J.; Kebreab, E.; Waghorn, G.; Makkar, H.P.S.; Adesogan, A.T.; Yang, W.; Lee, C.; Gerber, P.J.; Henderson, B.; Tricarico, J.M. Special topics – Mitigation of methane and nitrous oxide emissions from animal operations: I. A review of enteric methane mitigation options. *J. Anim. Sci.* **2013**, *91(11)*, pgs. 5045-69. https://10.2527/jas.2013-6583.
39. Carslaw, D.C.; Beevers, S.D.; Ropkins, K.; Bell, M.C. Detecting and quantifying aircraft and other on-airport contributions to ambient nitrogen oxides in the vicinity of a large international airport. *Atmospheric Environment* **2006**, *40(28)*, pgs. 5424-5434. https://doi.org/10.1016/j.atmosenv.2006.04.062.
40. Carslaw, D.C.; Beevers, S.D. Characterising and understanding emission sources using bivariate polar plots and k-means clustering. *Environmental Modelling & Software* **2013**, *40*, pgs. 325-329. https://doi.org/10.1016/j.envsoft.2012.09.005.
41. Lee, D.S.; Fahey, D.; Forster, P.M.; Newton, P.J.; Wit, R.C.N.; Lim, L.L.; Owen, B.; Sausen, R. Aviation and global climate change in the 21st century. *Atmos. Environ.* **2009**, *43*, pgs. 3520–3537. https://doi.org/10.1016/j.atmosenv.2009.04.024.
42. Lee, D.S.; Fahey, D.W.; Skowron, A.; Allen, M.R.; Burkhardt, U.; Chen, Q.; Doherty, S.J.; Freeman, S.; Forster, P.M.; Fuglestvedt, J.; Gettelman, A.; DeLeón, R.R.; Lim, L.L.; Lund, M.T.; Millar, R.J.; Owen, B.; Penner, J.E.; Pitari, G.; Prather, M.J.; Sausen, R.; Wilcox, L.J. The contribution of global aviation to anthropogenic climate forcing for 2000 to 2018. *Atmos. Environ.* **2021**, *244*, 117834. https://doi.org/10.1016/j.atmosenv.2020.117834.
43. Grobler, C.; Wolfe, P.J.; Dasadhikari, K.; Dedoussi, I.C.; Allroggen, F.; Speth, R.L.; Eastham, S.D.; Agarwal, A.; Staples, M.D.; Sabnis, J.; Barrett, S.R.H. Marginal climate and air quality costs of aviation emissions. *Environ. Res. Lett.* **2018**, *14*, 114031. https://doi.org/10.1088/1748-9326/ab4942.
44. Quadros, F.D.A.; Snellen, M.; Dedoussi, I.C. Regional sensitivities of air quality and human health impacts to aviation emissions. *Environ. Res. Lett.* **2020**, *15*, 105013. https://doi.org/10.1088/1748-9326/abb2c5.
45. Barrett, S.R.H.; Britter, R.E.; Waitz, I.A. Global Mortality Attributable to Aircraft Cruise Emissions. *Environ. Sci.* **2010**, *44*, 19, pgs. 7736–7742. https://doi.org/10.1021/es101325r.
46. Yim, S.H.L.; Lee, G.L.; Lee, I.H.; Allroggen, F.; Ashok, A.; Caiazzo, F.; Eastham, S.D.; Malina, R.; Barrett, S.R.H. Global, regional and local health impacts of civil aviation emissions. *Environ. Res. Lett.* **2015**, *10*, 3, 034001. https://doi.org/10.1088/1748-9326/10/3/034001.
47. Wild, O.; Prather, M.J.; Akimoto, H. Indirect long-term global radiative cooling from NO_x emissions. *Geophys. Res. Lett.* **2001**, *28*, pgs. 1719–1722. https://doi.org/10.1029/2000GL012573.
48. Stevenson, D.S.; Doherty, R.M.; Sanderson, M.G.; Collins, W.J.; Johnson, C.E.; Derwent, R.G. Radiative forcing from aircraft NO_x emissions: Mechanisms and seasonal dependence. *J. Geophys. Res. Atmospheres* **2004**, *109*, D17307. https://doi.org/10.1029/2004JD004759.
49. McNorton, J.; Bousserez, N.; Agustí-Panareda, A.; Balsamo, G.; Cantarello, L.; Engelen, R.; Huijnen, V.; Inness, A.; Kipling, Z.; Parrington, M.; Ribas, R. Quantification of methane emissions from hotspots and during COVID-19 using a global atmospheric inversion. *Atmos. Chem. Phys.* **2022**, *22(9)*, pgs. 5961–5981. https://doi.org/10.5194/acp-22-5961-2022.
50. Feng, L.; Palmer, P.I.; Parker, R.J.; Lunt, M.F.; Bösch, H. Methane emissions are predominantly responsible for record-breaking atmospheric methane growth rates in 2020 and 2021. *Atmos. Chem. Phys.* **2023**, *23*, pgs. 4863–4880. https://doi.org/10.5194/acp-23-4863-2023.